University of Windsor
Scholarship at UWindsor

Chemistry and Biochemistry Publications

Department of Chemistry and Biochemistry

2016

Transparent, Stretchable, and Conductive SWNT Films Using Supramolecular Functionalization and Layer-by-Layer Self-Assembly

Tricia B. Carmichael
University of Windsor

Akhil Vohra
University of Windsor

R. Stephen Carmichael
University of Windsor

Patigul Imin
McMaster University

Mokhtar Imit
McMaster University

See next page for additional authors

Follow this and additional works at: http://scholar.uwindsor.ca/chemistrybiochemistrypub

Part of the Materials Chemistry Commons

Recommended Citation

Authors

Tricia B. Carmichael, Akhil Vohra, R. Stephen Carmichael, Patigul Imin, Mokhtar Imit, Jagan Singh Meena, and Alex Adronov

CrossMark
click for updates

Transparent, stretchable, and conductive SWNT films using supramolecular functionalization and layer-by-layer self-assembly†

Akhil Vohra,[a] Patigul Imin,[b] Mokhtar Imit,[b] R. Stephen Carmichael,[a] Jagan Singh Meena,[a] Alex Adronov*[b] and Tricia Breen Carmichael*[a]

We demonstrate films of single-walled carbon nanotubes (SWNTs) on the elastomer polydimethylsiloxane (PDMS) that are stretchable, conductive, and transparent. Our fabrication method uses the supramolecular functionalization of SWNTs with conjugated polyelectrolytes to generate aqueous dispersions of positively- and negatively-charged SWNTs, followed by layer-by-layer self-assembly onto a PDMS substrate. Adding bilayers of positively- and negatively-charged SWNTs to the surface causes the sheet resistance and the % transmittance of the film to both progressively decrease. The sheet resistance decreases sharply in the first five bilayers as the layer-by-layer process efficiently establishes the percolation network, whereas the % transmittance declines more gradually. Films with 25 bilayers are transparent (75% at 550 nm) and conductive (560 ± 90 Ω □$^{-1}$). The combination of electrostatic and π-stacking forces very effectively bind the SWNTs within the film, producing smooth film surfaces (root-mean-square roughness of 18 nm) and enabling the films to remain conductive up to 80% elongation. We demonstrate the use of the SWNT films as transparent conductive electrodes in light-emitting devices and as soft strain sensors that are both wearable and transparent.

Introduction

The transparent conductor indium tin oxide (ITO) is an essential component of a wide range of today's electronic devices, such as liquid-crystal displays, touch panels, and solar cells.[1–4] These devices are fabricated on rigid glass substrates; however, the ability to create transparent conductors that are soft and stretchable opens the way to exciting new applications that are lightweight, portable, conformable, and even wearable. ITO is a brittle ceramic that requires high-temperature annealing to achieve low sheet resistance, which makes it incompatible with elastomeric substrates and stretchable devices.[5] A major research focus, therefore, is the development of new transparent conductors that can be deposited on elastomers and support stretchable electronics.[6,7] New stretchable transparent conductors such as thin metal films,[8–10] conducting polymers,[11,12] silver nanowires (AgNWs),[13–16] graphene,[17,18] and carbon nanotubes[19–27] have led to compelling technology demonstrations ranging from intrinsically stretchable light-emitting devices[8,13,21,28] and solar cells,[29,30] to rather sophisticated conformable dynamic

camouflage skins[31,32] and transparent strain sensors.[26,27,33] As research on stretchable transparent conductors progresses, there is an increasing focus on practical concerns such as scalability, precise control over film properties, sustainability, and cost. Here, we demonstrate a fabrication method that addresses these concerns to produce films of single-walled carbon nanotubes (SWNTs) on the elastomer polydimethylsiloxane (PDMS) that are stretchable, conductive, and transparent. We supramolecularly modify SWNTs with conjugated polyelectrolytes (CPEs) to disperse them in water, thus avoiding the need for organic solvents, and then use these solutions in a layer-by-layer (LbL) deposition process onto the PDMS surface. LbL deposition provides fine control over the optical and electrical properties of the film because it builds the films one SWNT layer at a time; at the same time, this method is both scalable and low cost.

The intrinsic electronic and mechanical properties of SWNTs are ideal for stretchable and transparent conductors; however, the key to integrating these materials into stretchable electronics lies in designing a film formation process that both retains and capitalizes on these properties. The high intrinsic conductivity (10^4 to 10^6 S cm^{-1}), high current-carrying capacity (up to ∼10^9 A cm^{-2}), and high thermal stability (up to 3500 W m^{-1} K^{-1}) of SWNTs are well suited to electronic applications.[6,19,34,35] SWNTs also possess high stiffness and strength (Young's modulus ∼1–2 TPa; tensile strength 50 GPa);[19] thus, individual SWNTs are not intrinsically stretchable. Integrating these materials into stretchable electronics may seem

[a]Department of Chemistry and Biochemistry, University of Windsor, Windsor, Ontario, Canada. E-mail: tbcarmic@uwindsor.ca

[b]Department of Chemistry and Chemical Biology, McMaster University, Hamilton, Ontario, Canada

† Electronic supplementary information (ESI) available: Table of sheet resistance and % transmittance. See DOI: 10.1039/c6ra02629j

counterintuitive; however, networks of SWNTs can remain conductive with stretching because individual SWNTs slide against each other under strain.[7,19] Designing a process to form transparent, conductive, and stretchable SWNT films that take advantage of these electrical and mechanical properties begins with choosing a method to effectively disperse SWNTs in solution, which is necessary to produce a uniformly distributed SWNT network with low sheet resistance. SWNTs, however, have a strong tendency to aggregate in solution through intermolecular π–π interactions, leading to inhomogeneous SWNT films. Researchers have used ultrasonication to exfoliate SWNTs in the presence of stabilizing surfactants,[7,36] and deposited the resulting dispersions on PDMS by spray-coating or Meyer rod coating to produce stretchable, transparent, and conductive films. These films have been implemented in pressure and strain sensors, and used as electrodes in stretchable light-emitting devices.[21,27,37] Although ultrasonication effectively disperses SWNTs, the downside is that it can disrupt π-conjugation of the SWNTs by introducing defects and dangling bonds to the sidewalls, thus diminishing the intrinsic conductivity.[38] Another approach avoids the dispersion problem altogether by directly drawing out solid nanotube films from aligned SWNT or multi-walled carbon nanotubes (MWNT) forests to generate stretchable, transparent, and conductive freestanding nanotube films, which may be transferred to a PDMS substrate.[39] These stretchable conductors have been employed as stretchable loudspeakers, wearable strain sensors, and touch panels.[22–26] Using SWNT films as transparent electrodes in thin-film devices such as light emitting electrochemical cells (LEECs) or organic light emitting diodes (OLEDs) presents another challenge: for these applications, the roughness of the transparent electrode surface must be <100 nm to prevent penetration of protruding SWNTs through overlying thin films, which can cause device shorting.[40–42] Embedding SWNT films in a polymer matrix can reduce the surface roughness from >60 nm for drop-cast films to <10 nm, providing smooth, transparent, and conductive SWNT films that have been used as electrodes in stretchable light-emitting electrochemical cells (LEECs).[21]

The excellent electrical and mechanical qualities of SWNTs are accompanied by disadvantageous optical properties: SWNTs are strong absorbers of visible light; in fact, the absorbance of vertically aligned SWNT forests (0.98–0.99) throughout the visible spectrum approaches that of an ideal black body.[43] Materials and methods to fabricate transparent conductors always face a trade-off between conductivity and transparency. Typically, increasing the thickness of a film increases the conductivity, yet decreases the transparency. The unfavorable optical properties of SWNTs suggest that nanoscale control of the film structure and thickness is crucial to produce a strong network for high conductivity while simultaneously maximizing the film transparency. One approach to achieve such control is LbL self-assembly, in which the deposition of alternating layers of oppositely charged materials onto a substrate builds up thin films one molecular layer at a time.[44–46] This method yields conformal, uniform thin films with fine control over the film thickness and architecture. Carbon nanotubes have been integrated in LbL fabrication schemes by first covalently bonding

charged functionalities directly to the nanotube sidewall, and then alternating the deposition of the functionalized nanotubes with either polymers or nanotubes functionalized with the opposite charge.[47–50] This methodology has been used to prepare sensors and thin-film electrodes on rigid glass substrates.[47–49,51] Similar to the exfoliation process by ultrasonication, however, the covalent modification process disrupts the π-conjugation of the nanotubes and diminishes the intrinsic conductivity.[6,7,52] As a result, researchers have turned to supramolecular functionalization of SWNTs as a non-destructive alternative. Supramolecular functionalization uses van der Waals and π–π interactions to non-covalently bind molecules or polymers to SWNT surfaces to solubilize SWNTs while preserving the nanotube structure, and thus the intrinsic electrical properties.[6,7,52,53] Shim *et al.* paired supramolecular functionalization with LbL self-assembly by wrapping SWNTs with charged aromatic polymers, and then alternating their deposition with polyelectrolytes to demonstrate transparent conductive electrodes on rigid glass substrates and free-standing films that were mechanically flexible. The process was not demonstrated on soft elastomeric substrates such as PDMS to enable stretchable transparent conductors.[54,55]

Here, we combine supramolecular functionalization and LbL self-assembly to fabricate transparent and conductive SWNT films that are also highly stretchable. We use water-soluble CPEs to generate aqueous dispersions of positively- and negatively-charged SWNTs, and use these in an LbL process on PDMS. The resulting films are transparent and stretchable, and remain conductive up to 80% elongation. This study also highlights a unique advantage of LbL self-assembly: the LbL process creates CPE–SWNT films that exhibit a low root-mean-square roughness (18 nm), making them candidates for transparent electrodes in thin-film devices. We demonstrate the key features of our CPE–SWNT films by using them as transparent electrodes in LEECs and as soft, wearable strain sensors to detect human motion.

Methods

CoMoCAT SWNTs (CG-200, SouthWest NanoTechnologies, Inc.), poly(dimethylsiloxane) (Sylgard 184, Dow Corning, Midland, MI), and poly(3,4-polyethylenedioxythiophene)-poly(styrenesulfonate) (PEDOT:PSS) (Clevios-P, Heraeus) were used as received. All other reagents were purchased commercially and used as received. SWNTs modified with poly[2,5-bis(3-sulfonatopropoxy)-1,4-ethynylphenylene-*alt*-1,4-ethynylphenylene] sodium salt (a-PPE–SWNTs)[53,56] and protonated poly[9,9-bis(diethylaminopropyl)-2,7-fluorene-*co*-1,4-phenylene] (PDAFP–SWNTs)[57] were prepared using previously published methods. Nanotube concentrations in the dispersions were estimated by UV-vis spectroscopic methods according to previously published procedures,[53] and were found to be approximately 1.5–2 mg mL^{-1}.

Preparation of activated PDMS substrates

PDMS substrates were prepared by casting a 10 : 1 w : w ratio of prepolymer : curing agent against polystyrene Petri dishes and curing at 60 °C for 1 h, and then treated with air plasma

(Harrick Plasma PDC32-G) at medium discharge setting for 40 seconds at an air pressure of 10 psig (flow rate of 32 mL min^{-1}). The oxidized substrates were then soaked for 10 min in a 1% (v/v) aqueous solution of 3-aminopropyltriethoxysilane (APTES), rinsed with distilled water, and then immersed in 6 M HCl for 1 min. The samples were then rinsed with distilled water and dried under a stream of nitrogen.

LbL self-assembly of CPE–SWNTs

Aqueous dispersions of a-PPE–SWNTs and PDAFP–SWNTs were sonicated in a Branson sonicator (Model 3510) for 1 min prior to LbL self-assembly. 2 mL of the a-PPE–SWNT dispersion was deposited on the activated PDMS substrate for 1 min, followed by rinsing with distilled water and drying under a stream of nitrogen. The surface was then treated with the aqueous solution of PDAFP–SWNTs using the same process. The process was repeated to form films with up to 25 bilayers of anionic a-PPE–SWNTs and cationic PDAFP–SWNTs.

LEEC fabrication

Devices were fabricated on both ITO-coated glass substrates (15–25 Ω □$^{-1}$, Delta Technologies) and 25-bilayer CPE–SWNT films on PDMS (25 bilayers). ITO-coated glass substrates were cleaned by sonication in deionized H$_2$O and isopropanol for 15 min each, followed by treatment with UV ozone cleaner (Jelight, Model no. 42A) for 5 min. CPE–SWNT films on PDMS were oxidized for 30 s in an air plasma (air pressure of 10 psig, flow rate 32 mL min^{-1}) at medium discharge setting. 0.7 mL of the PEDOT:PSS dispersion in water was sonicated for 15 min and then diluted by adding 0.3 mL of isopropanol; this solution was then spin-coated on the surface of either the ITO or CPE–SWNT film at 1000 rpm for 1 min. The PEDOT:PSS layers on ITO films and CPE–SWNT films were then annealed on a hot plate at 100 °C for 20 min. After cooling to room temperature, a Ru(dtb-bpy)$_3$(PF$_6$)$_2$/PDMS emissive layer[8] was deposited by spin-coating a 3 : 1 v : v mixture of a 40 mg mL^{-1} solution of Ru(dtb-bpy)$_3$(PF$_6$)$_2$ in dichloromethane and a 25 mg mL^{-1} solution of PDMS pre-polymer at 1000 rpm for 30 s, and then annealed in an oven at 60 °C overnight. A eutectic gallium–indium (EGaIn) cathode (50 μL) was deposited onto the surface of the Ru/PDMS film using a micropipette and then sealed in epoxy resin.

Strain sensor fabrication

CPE–SWNT films on PDMS (25 bilayers) were mounted to the back of an adhesive bandage using PDMS pre-polymer as the adhesive, followed by curing at 60 °C for one h. Connectors were fabricated by gluing strips of aluminum foil to the ends of the CPE–SWNT films using a conductive silicone paste (Effective Shielding, West Chester PA).
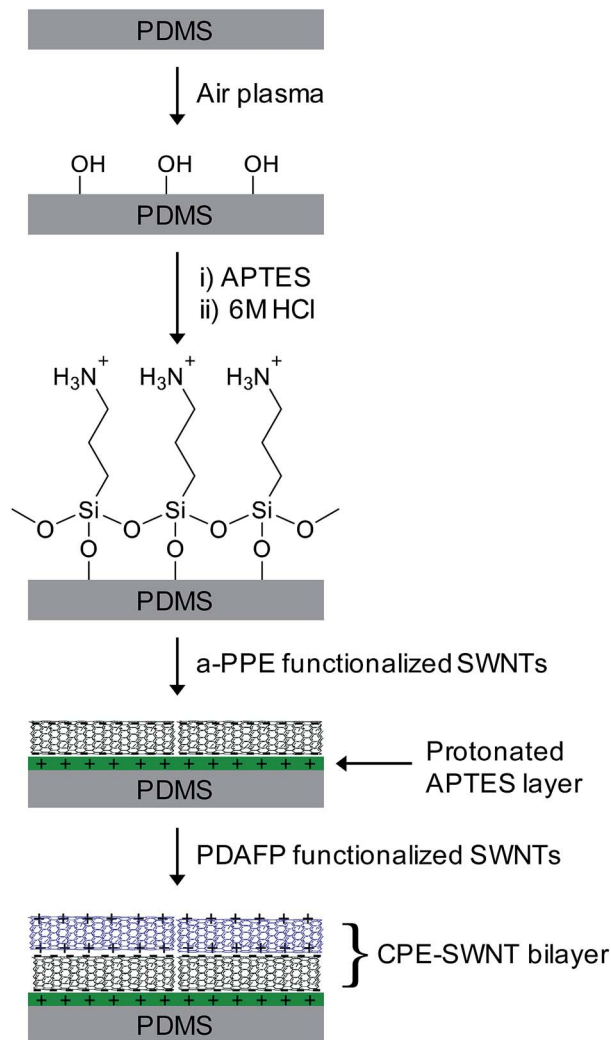
Characterization

Scanning electron microscope (SEM) images were obtained using an FEI Magellan Extreme High Resolution Field Emission Scanning Electron Microscope (XHR 400 FE-SEM). The voltage was 1.0 keV and a through the lens detector (TLD) was used. Transmission spectra were collected using a CARY 50 Conc UV-vis spectrophotometer. Electrical characterization was performed using a Keithley 2601A source meter. EGaIn (~0.01 mL) was first deposited by syringe to the corners (for sheet resistance measurements) or ends (for resistance measurements) of the CPE–SWNT surfaces to facilitate electrical contact. For electrical measurements under strain, samples were clamped in a microvice stretcher (S.T. Japan, USA, Inc.) and the resistance was measured at 5% increments of strain. Data sets consisted of a minimum of three samples, and the average was reported. AFM images were obtained using the dynamic force mode of a Park Systems XE-100 AFM (Surface Science Western, London, ON, Canada). A silicon cantilever with a nominal spring constant of 40 N m^{-1}, resonant frequency of 300 kHz and tip radius of 10 nm was used. Images were collected from three spots on each sample in an area of 40 μm × 40 μm, and processed using WSxM 5.0 Develop 8.0 software.[58] LEEC devices were characterized using a Keithley 2601 source-measure unit to apply a dc voltage and measure the current. Radiance was measured with a calibrated UDT S470 optometer attached to an integrating sphere.

Results and discussion

We used SWNTs functionalized with anionic and cationic CPEs to assemble SWNT–CPE films onto a charged PDMS surface one layer at a time. We chose anionic a-PPE and cationic PDAFP as the CPEs, which interact with SWNTs *via* supramolecular π–π interactions to produce anionic and cationic supramolecular polymer-nanotube assemblies that can be easily dispersed in water. We assembled SWNT–CPE films from these aqueous dispersions onto an activated PDMS substrate according to Scheme 1. After oxidizing the PDMS surface with an air plasma to introduce hydroxyl functional groups, treatment with the organosilane 3-aminopropyltriethoxysilane (APTES) produces an amine-terminated surface. Protonating the amino groups with HCl produces a surface comprising positively-charged ammonium groups. This activated surface electrostatically binds the anionic a-PPE–SWNT by simply depositing the a-PPE–SWNT aqueous solution onto the activated PDMS surface for one minute, followed by rinsing with water. The deposition of this first CPE–SWNT layer creates a negatively charged surface; exposing this surface to the cationic PDAFP–SWNT aqueous dispersion deposits the second CPE–SWNT layer and completes the formation of a CPE–SWNT bilayer. We repeated the alternating deposition of a-PPE–SWNTs and PDAFP–SWNTs to generate a total of 25 bilayers on the PDMS surface.

As CPE–SWNT bilayers are built up on the PDMS surface, the sheet resistance (R_s) and % transmittance both progressively decrease; however, they do not decrease at the same rate. Scanning electron microscopy (SEM) of a single bilayer CPE–SWNT film (Fig. 1) shows a sparse, porous network of CPE–SWNTs on the PDMS surface. The low density of CPE–SWNTs in the film produces a weak percolation network with an R_s value of 153 ± 25 kΩ □$^{-1}$ and a transmittance (98.3% at 550 nm) that is only slightly decreased from that of native PDMS

Scheme 1 Schematic illustration of LbL self-assembly of CPE-functionalized SWNTs on PDMS.

Fig. 1 SEM image of PDMS with a single bilayer of anionic a-PPE–SWNTs and cationic PDAFP–SWNTs.

Fig. 2 Electrical and optical properties of CPE–SWNT films on PDMS. (a) Plot of sheet resistance *versus* the number of CPE–SWNT bilayers on PDMS. (b) Transmittance spectra. Numbers in italics indicate the number of bilayers.

(100%). The variability in the R_s value may be attributed to the random mechanism of formation of the percolation network. Increasing the number of bilayers on the surface increases the number of possible SWNT–SWNT connections, thus providing more parallel pathways for current. The plot in Fig. 2a and data in Table S1† show that R_s decreases substantially by 88% ($\sim$135 kΩ $\square^{-1}$) between a single bilayer and five bilayers, followed by a gradual decline of only 10% over the remaining 20 bilayers. The initial precipitous drop in R_s between one and five bilayers contrasts with a relatively modest drop in transmittance of only $\sim$4%. Furthermore, the transmittance decreases by approximately the same amount every five bilayers (Fig. 2b). The fact that these two key film parameters do not decrease in tandem speaks to the efficiency of the LbL assembly process. The transmittance decreases regularly, indicating that the deposition process is well behaved: at each five-bilayer interval, the consistent decrease in transparency implies that every iteration of the LbL process adds an approximately equivalent amount of matter. However, each bilayer does not contribute equally to reducing R_s. In the initial five bilayers, the
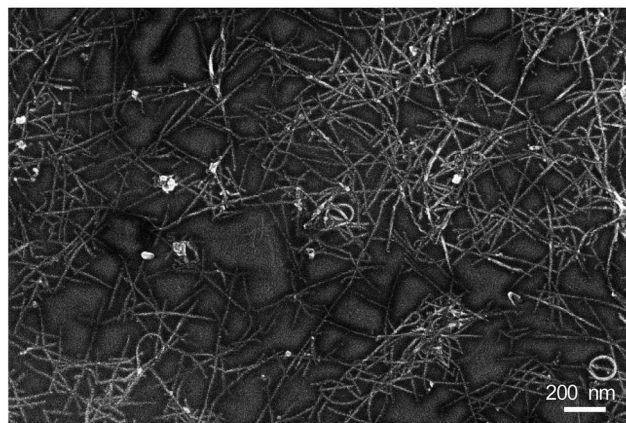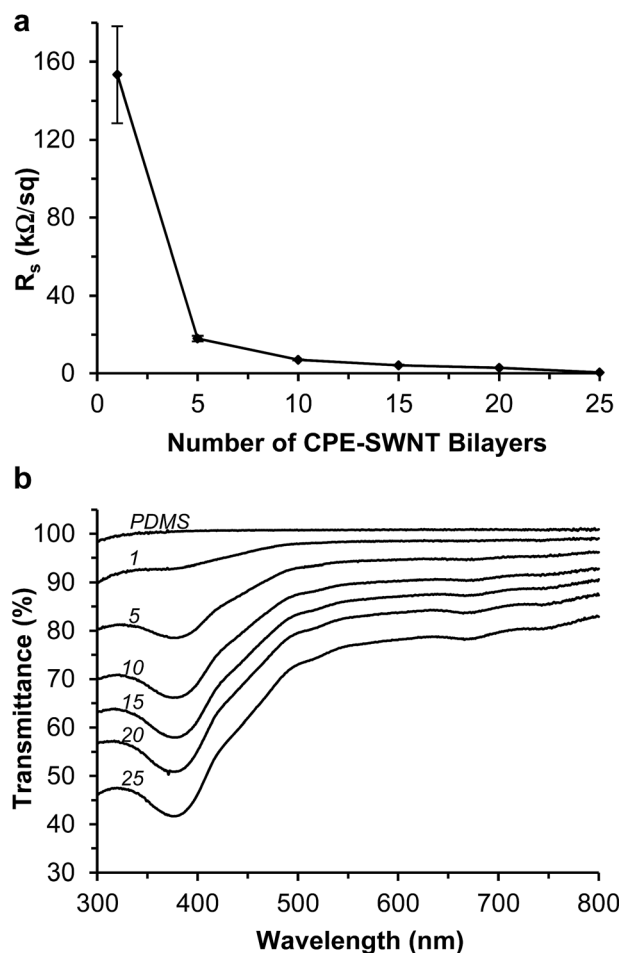
added CPE–SWNTs form SWNT–SWNT connections that efficiently construct the percolation network. Each of these bilayers contributes additional conductors in a random pattern that

may add additional conduction paths or reinforce existing paths, resulting in this initial dramatic decrease of R_s. At the same time, there are inevitable junction resistances introduced with each new SWNT–SWNT connection that become more relevant as more bilayers are added. This junction resistance is due to imperfect SWNT–SWNT contacts, particularly between metallic and semiconducting tubes,[59] which are likely furthermore influenced by the dielectric CPE shell around the SWNTs. After five bilayers, the benefit of adding more CPE–SWNTs to create more conduction pathways is nearly balanced by the penalty of additional junction resistances; thus, R_s declines marginally. By 25 bilayers, additional bilayers do not measurably decrease R_s. At this point, the films are analogous to a bulk material in which the conductivity is limited by the intrinsic junction resistance as well as the types of SWNTs in the film (a mixture of chiralities that are both metallic and semiconducting).

We chose to focus on 25-bilayer films for our study of the electrical and mechanical properties of CPE–SWNT films (Fig. 3a). 25-Bilayer films provide the lowest achievable R_s ($560 \pm 90 \ \Omega \ \square^{-1}$) while maintaining a transparency of 77% at 550 nm. Furthermore, we expect these films to have the highest number of SWNT–SWNT contacts – and thus redundant conduction paths – available to preserve conductivity when these structures are stretched. Despite the inclusion of the CPE in these films, the sheet resistance and % transmission of 25-bilayer films compare quite favorably to other stretchable transparent carbon nanotube films recently reported in the literature: SWNT films embedded at the surface of PDMS ($564 \ \Omega \ \square^{-1}$, 65% transparent);[33] SWNT films embedded at the surface of a polyacrylate stretchable above its glass transition temperature of 70 °C ($500 \ \Omega \ \square^{-1}$, 87% transparent);[21] carbon nanotubes spray-coated onto the surface of PDMS ($328 \ \Omega \ \square^{-1}$, 79% transparent);[27] carbon nanotube films transferred to the surface of Dragon Skin elastomer ($500 \ \Omega \ \square^{-1}$, 90% transparent);[26] and freestanding carbon nanotube films not integrated with an elastomeric substrate ($1 \ k\Omega \ \square^{-1}$, 78% transparent).[25]

SEM and atomic force microscopy (AFM) images of 25-bilayer CPE–SWNT films reveal that these films also possess smooth surfaces (Fig. 3 and 4), a feature that is essential to their use as stretchable transparent electrodes in thin-film devices. SEM images further show a dense, interconnected network of CPE–SWNTs that is ~200 nm thick with a smooth surface (Fig. 3b and c). Analysis of AFM images (Fig. 4) yields an RMS roughness of 18 ± 1 nm and a maximum peak-to-valley distance of 70 nm. The absence of CPE–SWNTs protruding from the film surface in the SEM and AFM images is consistent with a self-assembly process in which CPE–SWNTs in solution assemble in a "lying down" configuration to maximize favorable intermolecular electrostatic forces and π-stacking interactions. As a result, the RMS roughness of CPE–SWNT films is 70% lower than that of SWNT films formed by drop-casting (RMS roughness = 60 nm). The electrostatic and π-stacking interactions of CPE–SWNT films are also strong enough to render them durable to physical marring. There was a negligible change in R_s ($620 \pm 140 \ \Omega \ \square^{-1}$) of 25-bilayer CPE–SWNT films after vigorous agitation with a gloved finger for 10 s.
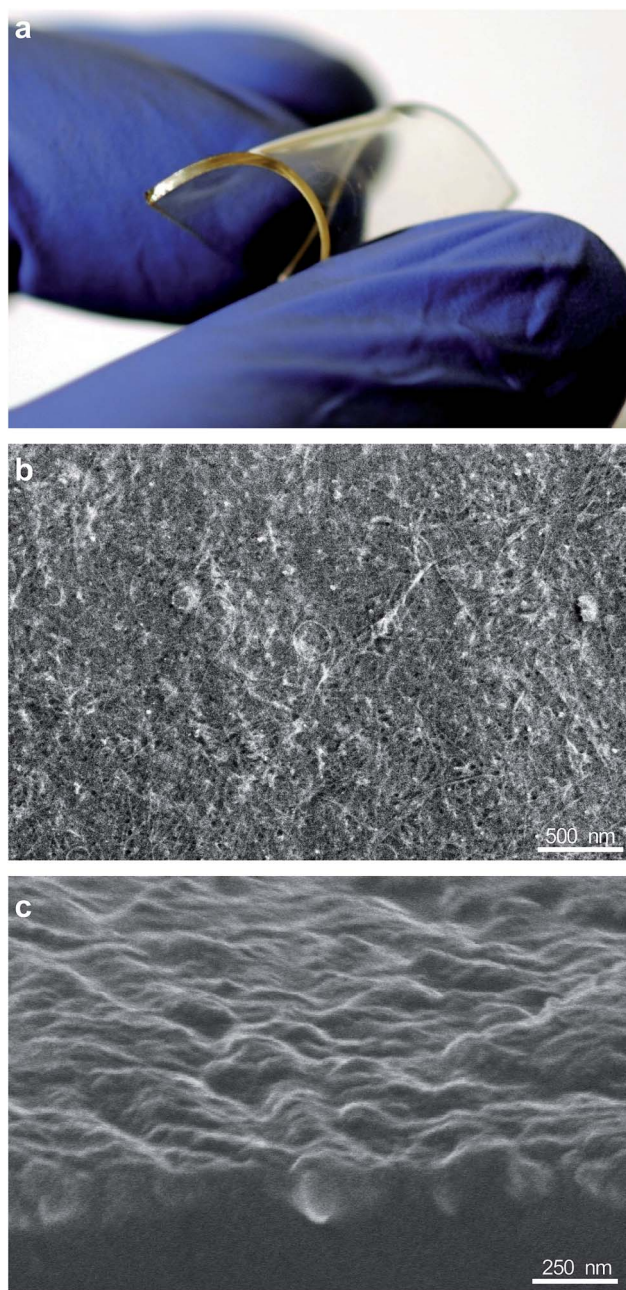
Fig. 3 25-Bilayer CPE–SWNT films on PDMS. (a) Photograph. (b) SEM image (top view). (c) SEM image (cross-section).

Surface roughness is a fundamentally important parameter of electrodes in thin-film devices. Protrusions from nanostructured electrodes can cause device shorting by producing localized regions of high electric fields or penetrating through an overlying device thin film.[40–42] Most reports of stretchable and transparent carbon nanotube films in the literature have not included surface roughness characterization. These films are typically studied as pressure, strain, and touch sensors for which surface roughness is not an important parameter. There is only one report in the literature of a stretchable and transparent carbon nanotube film employed in a thin-film light-emitting device, in which carbon nanotube films with
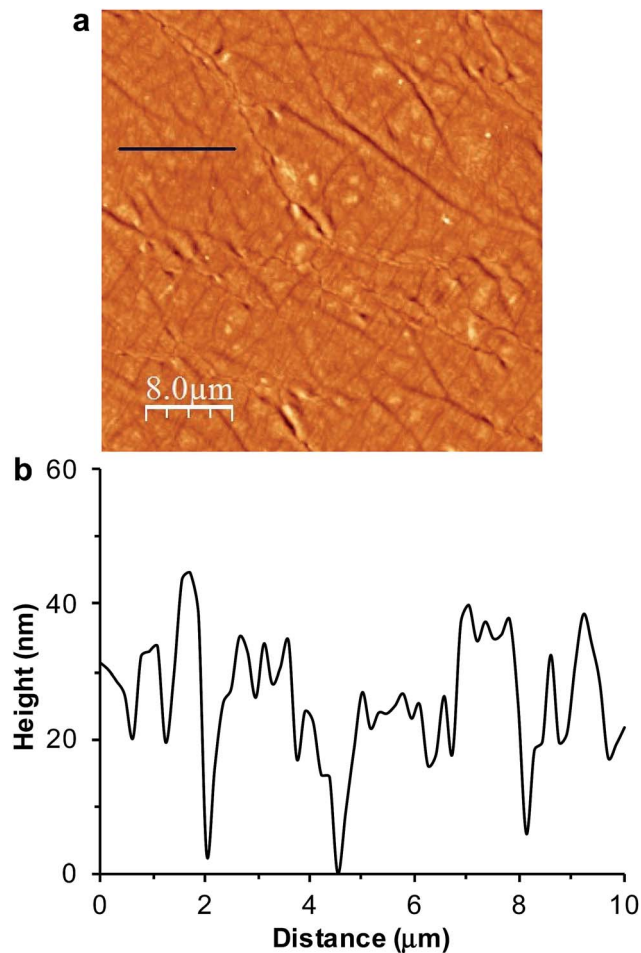
Fig. 4 Surface topography of 25-bilayer CPE–SWNT film on PDMS. (a) AFM image. (b) AFM profile corresponding to the section denoted by the black line in part (a).

low surface roughness were fabricated by embedding nanotubes into a polyacrylate and used as transparent electrodes in polymer light-emitting electrochemical cells (PLECs). Heating the PLECs above the glass transition temperature of the polyacrylate (70 °C) produced an intrinsically stretchable thin-film device.[21] We used a proof-of-concept demonstration to show that the low surface roughness of 25-bilayer CPE–SWNT films on PDMS makes them viable as transparent electrodes by implementing them in thin-film LEEC devices. LEECs are simple devices that consist of an anode and cathode sandwiched around an emissive layer.[60,61] We used the ionic transition metal complex, $Ru(dtb-bpy)_3(PF_6)_2$ as the emissive material. $Ru(dtb-bpy)_3(PF_6)_2$ supports charge injection and transport in the device, as well as emissive recombination to produce 630 nm light.[60] We fabricated LEECs by spin-coating a layer of PEDOT:PSS as a hole transport layer on the CPE–SWNT film on PDMS to construct the transparent anode, followed by spin-coating a layer of $Ru(dtb-bpy)_3(PF_6)_2$ dispersed in a PDMS polymer matrix to improve the uniformity of the film. We used a drop of liquid EGaIn on the surface as the cathode to complete the device. Applying a dc voltage of 40 V to the devices

resulted in the emission of light (Fig. 5a), which we recorded over a 30 minute testing period. The evolution of current and radiance (Fig. 5a) and external quantum efficiency (EQE) (Fig. 5b) show that the devices reach their maximum EQE of 0.004% at 116 s. The continuous operation of these devices for 30 minutes – with no evidence of electrical shorts – verifies that CPE–SWNT films on PDMS are viable transparent electrodes for thin-film devices. However, the EQE of LEECs with a CPE–SWNT electrode is lower than that of analogous devices in which the CPE–SWNT electrode is replaced by a standard ITO electrode and coated with PEDOT:PSS (EQE = 0.01 ± 0.002). We expect that the device properties of CPE–SWNT LEECs can be improved by making the electric field at the anode more uniform. Uniformity of the electric fields at the electrodes is essential for optimal device operation and good device efficiencies due to the electrochemical doping process that is central to the operating mechanism of LEECs.[61–65] Upon application of a voltage, the PF_6^- counterions migrate under the influence of the electric field to the anode interface, leaving uncompensated metal ions near the cathode. The accumulation and depletion of PF_6^- counterions produce high electric fields near the electrode interfaces, lowering the barrier to charge injection. Charge injection reduces Ru^{2+} ions adjacent to the cathode and oxidizes Ru^{2+} ions adjacent to the anode; subsequent charge hopping creates an emissive zone of adjacent Ru^+ and Ru^{3+} ions, which undergo a recombinative process with
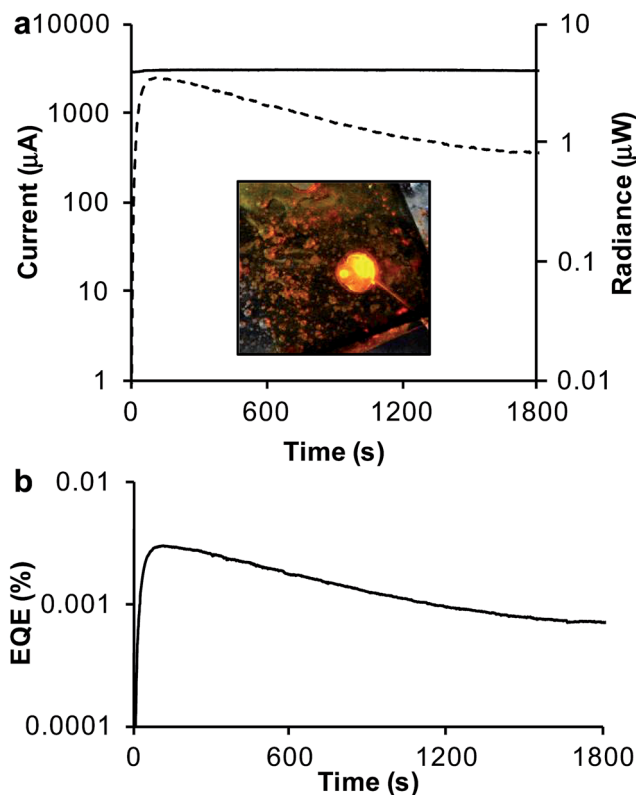

Fig. 5 Demonstration of 25-bilayer CPE–SWNT films on PDMS as transparent anodes in LEECs. Evolution of (a) current (solid line) and radiance (dotted line) and (b) EQE over a 30 minute testing period. Inset in (a) is a photograph of an operating LEEC.

visible light emission.[60] Our CPE–SWNT films are composed of a mixture of semiconducting and metallic nanotubes; therefore, the electric field generated at the film surface is inherently non-uniform due to the differing conductivities of the SWNTs compared to the electric field generated at the surface of a uniformly conductive electrode such as ITO. As a result, the emissive zone of CPE–SWNT devices will be less coherent. To improve the properties of LEECs formed using CPE–SWNT electrodes, it will thus be necessary to improve the homogeneity of the electric field generated at the electrode surface by creating CPE–SWNT films from a single type of nanotube – either purely metallic or purely semiconducting – rather than a mixture of metallic and semiconducting SWNTs. An attractive option would be to combine semiconductor-enriched CPE–SWNT films with redox doping. The uniformly conductive SWNTs comprising these films would produce a homogeneous electric field to improve the device properties of LEECs, and may give the added benefit of improving the conductivity of CPE–SWNT electrodes: Blackburn *et al.* reported the main resistance in semiconductor-enriched SWNT films – the contact resistance of the intertube junctions – can successfully be reduced using redox doping to increase the delocalized carrier density and transmission probability through SWNT–SWNT junctions. This process is more effective for semiconductor-enriched films than for metal-enriched films.[66]

In general, the resistance of SWNT films increases with stretching, which can be attributed to the separation of SWNT–SWNT junctions as a result of elongation. The magnitude of the resistance increase and the recovery of conductivity upon releasing the strain depend on the properties of the SWNT film. SWNT films deposited on top of elastomers may experience delamination, which can lead to irreversible loss of conductivity; embedding SWNTs into polymers is regarded as a way to avoid this critical problem. Despite the fact that 25-bilayer CPE–SWNT films are not mechanically stabilized by embedment in a polymer matrix, the combination of electrostatic and π-stacking interactions are strong enough to stabilize these films to stretching, enabling them to remain conductive to high elongations (up to 80%) and largely recover conductivity when the strain is released. The normalized change in resistance (R/R_0) as a function of elongation of 25-bilayer CPE–SWNT is plotted in Fig. 6a. The resistance increases relatively linearly with strain, and reaches 12.3 times the initial value (R_0) at 80% elongation. Fracture of the samples occurs beyond 80% elongation, suggesting that it may be possible to prepare conductive CPE–SWNT films that function at even higher strains by using an elastomer with a higher tensile strength than PDMS. Elongating CPE–SWNT films to 80% and then returning to 0% strain restores the conductivity of the film to an R/R_0 recovery value of 1.6 ± 0.2. We attribute this recovery to the ability of the electrostatic and π-stacking interactions to mechanically stabilize the CPE–SWNTs in the film and allow them to reconnect, although this value is also consistent with a small, irrecoverable loss of SWNT–SWNT junctions. The electrostatic and π-stacking forces of 25-bilayer CPE–SWNT films are also sufficient to stabilize these films to repetitive stretch-release cycles. We subjected 25-bilayer CPE–SWNT films on PDMS to cycles of 15%
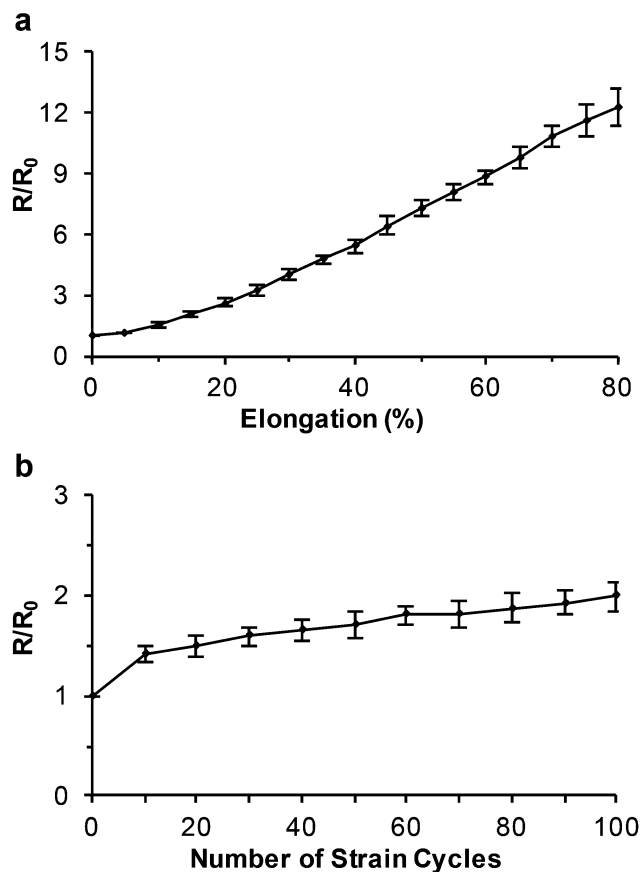

Fig. 6 25-Bilayer CPE–SWNT films on PDMS subjected to stretching. (a) Change in resistance as a function of elongation. (b) Change in resistance as a function of the number of 15% strain cycles.

strain, and measured the resistance in the relaxed state (at 0% strain) after every 10 cycles. Plots of the resistance change *versus* the number of strain cycles (Fig. 6b) show that R/R_0 remained relatively constant (<2) throughout the testing range of 100 cycles, although the slight gradual increase in R/R_0 suggests some loss of SWNT–SWNT junctions.

Strain sensors fabricated using soft, conformable materials can be worn on the body to quantify human motion through changes in electrical resistance. The characteristics of an ideal human motion strain sensor include high stretchability, high sensitivity, excellent stability, and tolerance to repetitive strain.[67] Hard sensors such as metal foils or inorganic semiconductors are widely used to sense structural changes or deformation in stiff materials, such as buildings or aircraft. These sensors provide a range of sensitivities, which are quantified by the gauge factor, the ratio of the fractional change in resistance ($\Delta R/R_0$) to mechanical strain ε.

$$GF = \frac{\Delta R/R_0}{\varepsilon}$$

Metal strain gauges, with their low gauge factors of 2–5, are used to detect gross deformations, whereas semiconductor strain gauges are useful for precision measurements due to their high gauge factors (up to 200).[68–70] These useful
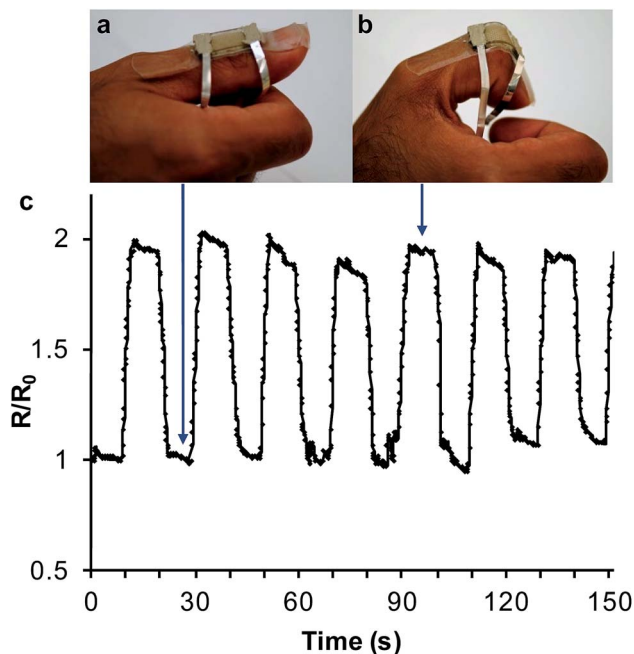
Fig. 7 Demonstration of 25-bilayer CPE–SWNTs on PDMS as a wearable strain sensor. Photograph of the sensor mounted on a human thumb in (a) straightened (unstrained) and (b) bent (strained) positions. (c) Plot of normalized resistance as a function of time corresponding to bending/straightening cycles.

Bending the thumb caused a resistance change of ~2× the initial value, which corresponds to ~15% strain on the line of best fit of the R/R_0 vs. elongation plot in Fig. 6a. Straightening the thumb recovered the resistance to within 8% of the initial value. Based on Fig. 6a, CPE–SWNT films on PDMS are capable of detecting up to 80% strain, suggesting the potential to detect a broad range of human or robotic motion.

Conclusions

We have combined supramolecular functionalization of SWNTs with LbL self-assembly to fabricate transparent, stretchable, and conductive CPE–SWNT films on PDMS. The LbL process is green, scalable, and low cost, and it efficiently establishes the percolation network largely within the first five bilayers. We credit the smoothness and ability of our films to remain conductive with stretching to the combination of electrostatic and π-stacking forces, which very effectively bind the SWNTs within the film. The combination of properties exhibited by our CPE–SWNT films – conductivity, transparency, low surface roughness, and stretchability with low resistance changes – is what distinguishes our films from others reported in the literature. We have exploited this combination of properties to show that CPE–SWNT films are viable as transparent conductive electrodes in LEECs, and can also be applied as soft strain sensors that are both wearable and transparent. Our CPE–SWNT films are made from a mixture of semiconducting and metallic SWNTs, which may adversely affect the uniformity of the electric field generated at the surface due to the differing conductivities of the semiconducting and metallic SWNTs in the film. This non-uniform electric field is problematic when these films are employed as transparent electrodes in thin-film devices such as LEECs. Therefore, the next step in the development of CPE–SWNT films will be to improve the uniformity of the electric field generated at the surface. We aim to accomplish this improvement through redox doping of semiconductor-enriched CPE–SWNT films, which may also bring the added benefit of improving the film conductivity. We will report details of such optimized CPE–SWNT films and their use in stretchable devices in due course.

instruments are, however, entirely unsuitable to monitor human or even robotic motion, because they lack conformability and cannot function at high strains typical of, for example, the bending of an elbow joint. Intrinsically stretchable conductive materials, such as elastomers loaded with conductive particles or stretchable conductive films on elastomers, provide the softness and stretchability for these "soft" applications.[26,27,37,67,71–73] We fabricated wearable strain sensors from 25-bilayer CPE–SWNT films on PDMS for four reasons: first, CPE–SWNT films are soft and conformable, exhibit resistance changes with stretching to high elongations, and tolerate repeated deformation. Second, the gauge factor of these films determined from the slope of the line of best fit of the plot of R/R_0 vs. elongation in Fig. 6a is 15.0 for strains of 0–80%. This value is higher than the gauge factor of aligned SWNT films on PDMS, which decreases from 0.82 for strains of 0–40% to 0.06 for strains >40.[37] Third, the process to manufacture CPE–SWNT films on PDMS is low-cost, green (due to the aqueous CPE–SWNT dispersions), and scalable. Fourth, CPE–SWNT films are transparent. Adding transparency to strain sensors brings added functionality to motion detection, particularly in robotics, because these sensors can be integrated with on-board optoelectronic devices and can enable direct observation through the sensors.[26,27,33] To fabricate CPE–SWNT strain sensors, we glued a 25-bilayer CPE–SWNT/PDMS structure onto an adhesive bandage, and then simply adhered the bandage along the length of a human thumb. We then applied a voltage of 20 V and measured the change in resistance as the thumb was repeatedly bent and straightened at 10 s intervals (Fig. 7).

References

1 U. Betz, M. K. Olsson, J. Marthy, M. F. Escolá and F. Atammy, *Surf. Coat. Technol.*, 2006, **200**, 5751–5759.

2 E. Fortunato, D. Ginley, H. Hosono and D. C. Paine, *MRS Bull.*, 2007, **32**, 242–247.

3 W.-Y. Chang, H.-J. Lin and J.-S. Chang, *Opt. Lett.*, 2011, **36**, 894–896.

4 K. Schulze, B. Maennig, K. Leo, Y. Tomita, C. May, J. Hüpkes, E. Brier, E. Reinold and P. Bäuerle, *Appl. Phys. Lett.*, 2007, **91**, 073521.

5 B. G. Lewis and D. C. Paine, *MRS Bull.*, 2000, **25**, 22–27.

6 D. S. Hecht, L. Hu and G. Irvin, *Adv. Mater.*, 2011, **23**, 1482–1513.

7 J. Du, S. Pei, L. Ma and H.-M. Cheng, *Adv. Mater.*, 2014, **26**, 1958–1991.

8 H. L. Filiatrault, G. C. Porteous, R. S. Carmichael, G. J. E. Davidson and T. B. Carmichael, *Adv. Mater.*, 2012, **24**, 2673–2678.

9 C. F. Guo, Q. Liu, G. Wang, Y. Wang, Z. Z. Shi, Z. Suo, C.-W. Chu and Z. Ren, *Proc. Natl. Acad. Sci. U. S. A.*, 2015, **112**, 12332–12337.

10 C. F. Guo, T. Sun, Q. Liu, Z. Suo and Z. Ren, *Nat. Commun.*, 2014, **5**, 3121.

11 M. Vosgueritchian, D. J. Lipomi and Z. Bao, *Adv. Funct. Mater.*, 2012, **22**, 421–428.

12 D. J. Lipomi, J. A. Lee, M. Vosgueritchian, B. C.-K. Tee, J. A. Bolander and Z. Bao, *Chem. Mater.*, 2012, **24**, 373–382.

13 J. Liang, L. Li, X. Niu, Z. Yu and Q. Pei, *Nat. Photonics*, 2013, **7**, 817–824.

14 T. Akter and W. S. Kim, *ACS Appl. Mater. Interfaces*, 2012, **4**, 1855–1859.

15 W. Hu, X. Niu, L. Li, S. Yun, Z. Yu and Q. Pei, *Nanotechnology*, 2012, **23**, 344002.

16 T. Cheng, Y.-Z. Zhang, W.-Y. Lai, Y. Chen, W.-J. Zeng and W. Huang, *J. Mater. Chem., C*, 2014, **2**, 10369–10376.

17 X. Li, R. Zhang, W. Yu, K. Wang, J. Wei, D. Wu, A. Cao, Z. Li, Y. Cheng, Q. Zheng, R. S. Ruoff and H. Zhu, *Sci. Rep.*, 2012, **2**, 870.

18 K. S. Kim, Y. Zhao, H. Jang, S. Y. Lee, J. M. Kim, K. S. Kim, J.-H. Ahn, P. Kim, J.-Y. Choi and B. H. Hong, *Nat. Lett.*, 2009, **457**, 706–710.

19 Q. Cao and J. A. Rogers, *Adv. Mater.*, 2009, **21**, 29–53.

20 L. Hu, W. Yuan, P. Brochu, G. Gruner and Q. Pei, *Appl. Phys. Lett.*, 2009, **94**, 161108.

21 Z. Yu, X. Niu, Z. Liu and Q. Pei, *Adv. Mater.*, 2011, **23**, 3989–3994.

22 C. Feng, K. Liu, J.-S. Wu, L. Liu, J.-S. Cheng, Y. Zhang, Y. Sun, Q. Li, S. Fan and K. Jiang, *Adv. Funct. Mater.*, 2010, **20**, 885–891.

23 Y. Zhang, C. J. Sheehan, J. Zhai, G. Zou, H. Luo, J. Xiong, Y. T. Zhu and Q. X. Jia, *Adv. Mater.*, 2010, **22**, 3027–3031.

24 L. Cai, J. Li, P. Luan, H. Dong, D. Zhao, Q. Zhang, X. Zhang, M. Tu, Q. Zeng, W. Zhou and S. Xie, *Adv. Funct. Mater.*, 2012, **22**, 5238–5244.

25 L. Xiao, Z. Chen, C. Feng, L. Liu, Z.-Q. Bai, Y. Wang, L. Qian, Y. Zhang, Q. Li, K. Jiang and S. Fan, *Nano Lett.*, 2008, **8**, 4539–4545.

26 L. Cai, L. Song, P. Luan, Q. Zhang, N. Zhang, Q. Gao, D. Zhao, X. Zhang, M. Tu, F. Yang, W. Zhou, Q. Fan, J. Luo, W. Zhou, P. M. Ajayan and S. Xie, *Sci. Rep.*, 2013, **3**, 3048.

27 D. J. Lipomi, M. Vosgueritchian, B. C.-K. Tee, S. L. Hellstrom, J. A. Lee, C. H. Fox and Z. Bao, *Nature Nanotech.*, 2011, **6**, 788–792.

28 J. Wang, C. Yan, K. J. Chee and P. S. Lee, *Adv. Mater.*, 2015, **27**, 2876–2882.

29 D. J. Lipomi and Z. Bao, *Energy Environ. Sci.*, 2011, **4**, 3314–3328.

30 D. J. Lipomi, B. C.-K. Tee, M. Vosgueritchian and Z. Bao, *Adv. Mater.*, 2011, **23**, 1771–1775.

31 Q. Wang, G. R. Gossweiler, S. L. Craig and X. Zhao, *Nat. Commun.*, 2014, **5**, 4899.

32 H.-H. Chou, A. Nguyen, A. Chortos, J. W. F. To, C. Lu, J. Mei, T. Kurosawa, W.-G. Bae, J. B.-H. Tok and Z. Bao, *Nat. Commun.*, 2015, **6**, 8011.

33 X. Wang, T. Li, J. Adams and J. Yang, *J. Mater. Chem. A*, 2013, **1**, 3580–3586.

34 Z. Yao, C. L. Kane and C. Dekker, *Phys. Rev. Lett.*, 2000, **84**, 2941–2944.

35 T. W. Ebbesen, H. J. Lezec, H. Hiura, J. W. Bennett, H. F. Ghaemi and T. Thio, *Nature*, 1996, **382**, 54–56.

36 G. J. Bahun and A. Adronov, *J. Polym. Sci., Part A: Polym. Chem.*, 2010, **48**, 1016–1028.

37 T. Yamada, Y. Hayamizu, Y. Yamamoto, Y. Yomogida, A. Izadi-Najafabadi, D. N. Futaba and K. Hata, *Nat. Nanotechnol.*, 2011, **5**, 296–301.

38 M. D. Rossell, C. Kuebel, G. Ilari, F. Rechberger, F. J. Heiligtag, M. Niederberger, D. Koziej and R. Erni, *Carbon*, 2013, **61**, 404–411.

39 K. Jiang, Q. Li and S. Fan, *Nature*, 2002, **419**, 801.

40 J.-Y. Lee, S. T. Connor, Y. Cui and P. Peumans, *Nano Lett.*, 2008, **8**, 689–692.

41 L. Hu, H. S. Kim, J.-Y. Lee, P. Peumans and Y. Cui, *ACS Nano*, 2010, **4**, 2955–2963.

42 K.-H. Ok, J. Kim, S.-R. Park, Y. Kim, C.-J. Lee, S.-J. Hong, M.-G. Kwak, N. Kim, C. J. Han and J.-W. Kim, *Sci. Rep.*, 2015, **5**, 9464.

43 J. Ishii, H. Kishida, Y. Hayamizu, S. Yasuda, D. N. Futaba, M. Yumura and K. Hata, *Proc. Natl. Acad. Sci. U. S. A.*, 2009, **106**, 6044–6047.

44 P. T. Hammond, *AIChE J.*, 2011, **57**, 2928–2940.

45 X. Zhang, H. Chen and H. Zhang, *Chem. Commun.*, 2007, 1395–1405.

46 K. Ariga, J. P. Hill and Q. Ji, *Phys. Chem. Chem. Phys.*, 2007, **9**, 2319–2340.

47 S. W. Lee, B.-S. Kim, S. Chen, Y. Shao-Horn and P. T. Hammond, *J. Am. Chem. Soc.*, 2009, **131**, 671–679.

48 M. N. Hyder, S. W. Lee, F. Ç. Cebeci, D. J. Schmidt, Y. Shao-Horn and P. T. Hammond, *ACS Nano*, 2011, **5**, 8552–8561.

49 J. R. Siqueira Jr, C. F. Werner, M. Bäcker, A. Poghossian, V. Zucolotto, O. N. Oliviera Jr and M. J. Schöning, *J. Phys. Chem. C*, 2009, **113**, 14765–14770.

50 T. Bohnenberger, L. D. Rafailovic, C. Weilach, D. Hubmayr and U. Schmid, *Thin Solid Films*, 2014, **551**, 68–73.

51 P. W. Barone, S. Y. Baik, D. A. Heller and M. S. Strano, *Nat. Mater.*, 2005, **4**, 86–92.

52 L. Hu, D. S. Hecht and G. Grüner, *Chem. Rev.*, 2010, **110**, 5790–5844.

53 F. Cheng, P. Imin, S. Lazar, G. A. Botton, G. de Silveira, O. Marinov, J. Deen and A. Adronov, *Macromolecules*, 2008, **41**, 9869–9874.

54 B. S. Shim, Z. Tang, M. P. Morabito, A. Agarwal, H. Hong and N. A. Kotov, *Chem. Mater.*, 2007, **19**, 5467–5474.

55 B. S. Shim, J. Zhu, E. Jan, K. Critchley and N. A. Kotov, *ACS Nano*, 2010, **4**, 3725–3734.

56 C. Y. Tan, M. R. Pinto and K. S. Schanze, *Chem. Commun.*, 2002, 446–447.

57 T. Casagrande, P. Imin, F. Cheng, G. A. Botton, I. Zhitomirsky and A. Adronov, *Chem. Mater.*, 2010, **22**, 2741–2749.

58 I. Horcas, R. Fernández, J. M. Gómez-Rodríguez, J. Colchero, J. Gómez-Herrero and A. M. Baro, *Rev. Sci. Instrum.*, 2007, **78**, 013705.

59 M. S. Fuhrer, J. Nygård, L. Shih, M. Forero, Y.-G. Yoon, M. S. C. Mazzoni, H. J. Choi, J. Ihm, S. G. Louie, A. Zettl and P. L. McEuen, *Science*, 2000, **288**, 494–497.

60 J. D. Slinker, J. Rivnay, J. S. Moskowitz, J. B. Parker, S. Bernhard, H. D. Abruña and G. G. Malliaras, *J. Mater. Chem.*, 2007, **17**, 2976–2988.

61 Q. Pei, G. Yu, C. Zhang, Y. Yang and A. J. Heeger, *Science*, 1995, **269**, 1086–1088.

62 M. Lenes, G. Garcia-Belmonte, D. Tordera, A. Pertegas, J. Bisquert and H. J. Bolink, *Adv. Funct. Mater.*, 2011, **21**, 1581–1586.

63 J. D. Slinker, J. A. DeFranco, M. J. Jaquith, W. R. Silveira, Y. W. Zhong, J. M. Moran-Mirabal, H. G. Craighead, H. D. Abruna, J. A. Marohn and G. G. Malliaras, *Nat. Mater.*, 2007, **6**, 894–899.

64 J. C. deMello, *Phys. Rev. B: Condens. Matter Mater. Phys.*, 2002, **66**, 235210.

65 D. B. Rodovsky, O. G. Reid, L. S. C. Pingree and D. S. Ginger, *ACS Nano*, 2010, **4**, 2673–2680.

66 J. L. Blackburn, T. M. Barnes, M. C. Beard, Y.-H. Kim, R. C. Tenent, T. J. McDonald, B. To, T. J. Coutts and M. J. Heben, *ACS Nano*, 2008, **2**, 1266–1274.

67 N. Lu, C. Lu, S. Yang and J. Rogers, *Adv. Funct. Mater.*, 2012, **22**, 4044–4050.

68 A. L. Window, *Strain Gauge Technology*, Springer, Netherlands, 1992.

69 C. S. Smith, *Phys. Rev.*, 1954, **94**, 42–49.

70 S. M. Sze, *Semiconductor Sensors*, Wiley, New York, 1994.

71 M. Amjadi, A. Pichitpajongkit, S. Lee, S. Ryu and I. Park, *ACS Nano*, 2014, **8**, 5154–5163.

72 C. S. Boland, U. Khan, C. Backes, A. O'Neill, J. McCauley, S. Duane, R. Shanker, Y. Liu, I. Jurewicz, A. B. Dalton and J. N. Coleman, *ACS Nano*, 2014, **8**, 8819–8830.

73 H. L. Filiatrault, R. S. Carmichael, R. A. Boutette and T. B. Carmichael, *ACS Appl. Mater. Interfaces*, 2015, **7**, 20745–20752.